Comparison of fluvial dike breaching numerical modelling approaches

V. Schmitz[1], P. Archambeau[1], M. Pirotton[1], S. Erpicum[1] & B. Dewals[1]
[1] *Research Group of Hydraulics in Environmental and Civil Engineering (HECE), University of Liège, Liège, Belgium.*

ABSTRACT: Failures of fluvial dikes often lead to devastating consequences in floodplains. Overtopping is the most frequent cause of dike failure. Numerical models are instrumental tools to assess the consequences of failure and guide emergency plans. Multiple modelling strategies exist regarding dike morphology and flow descriptions but also the coupling between them. The selected modelling strategy significantly influences the model accuracy and computational performance. Here, we compare the accuracy and performance of two modelling approaches against data from field experiments. The first modelling strategy consists in describing the flow and the morphologic evolution of the dike breach using a non-discretized dike breaching model. In the second modelling strategy, we use a dynamic coupling of a 2D hydrodynamic model with the breach evolution module of the non-discretized dike breaching model, whose goal is now limited to the description of the dike breach morphodynamics. Overall, numerical models perform well in the prediction of the breach discharge evolution. However, the breach evolution module of the non-discretized model highly underestimates the breach expansion and should thus be revised in further studies.

1 INTRODUCTION

With the surge of extreme meteorological events, intensification of urbanization in the floodplains and aging infrastructures, fluvial dikes get more and more prompt to breaching. Hence, the need for predictive dike breaching models has become of paramount importance for establishing safe land-use planning and emergency response procedures (Zhong et al., 2021). Multiple modelling strategies exist regarding dike morphology and flow descriptions. The selected strategy significantly influences the model accuracy and computational performance.

The simplest and most computational-efficient models do not require any discretization of the domain and are therefore called “lumped models”. Among this category, statistical (or parametric) models are exclusively based on regression analysis of data from past events, without considering underlying physics (De Lorenzo and Macchione, 2014; Chen et al., 2019; Lee, 2019). In contrast, lumped physics-based models enable simulating hydraulic and dike breach variables (e.g., time-evolution of breach discharge and dimensions) by describing selected physical processes (Wu, 2016; Peter et al., 2018; Tsai et al., 2019; Li et al., 2020; Van Damme, 2020). For this reason, they may be considered as more general and trustworthy than purely statistical models. Conversely to lumped models, fully distributed physically based models can describe the phenomenon in greater detail, as they solve the flow and sediment governing equations using a computational mesh of the domain (e.g., Dazzi et al. (2019) or Hu et al. (2023)). Provided that the correct physical processes (including geotechnical aspects, e.g., side slope collapses) are properly incorporated in the model structure, their results are expected to be more accurate than lumped models, to the expense of a substantial increase in their computational cost. Nevertheless, combining a spatially distributed sediment transport model of dike breaching and a hydrodynamic model is usually avoided. 2D models based on shallow-water equations can only represent horizontal

surface erosion, although geotechnical three-dimensional effects cannot be neglected. However, 3D models are computationally too demanding. Therefore, lumped models for dike breaching are often preferred. This coupling may be dynamic, i.e., data are shared between modules during computation, or static, i.e., the modules are run sequentially.

Here, we implemented two modelling strategies. The first modelling approach consists in describing the flow and the morphologic evolution of the dike breach using our adapted version of the lumped physically based model "DLBreach" (Schmitz et al., 2023) that was initially developed by Wu (2013) for dam breaching, i.e., frontal configuration. In the other modelling approach, we use a dynamic coupling of an in-house-developed 2D hydrodynamic model based on shallow-water equations (WOLF-2D) with our adapted dike breach mode, whose goal is now limited to the description of the dike breach morphodynamics.

Two experimental field tests led by Kakinuma et al. (2013) on a 735-m-long stretch of the Chiyoda Test Channel (Japan) are used to assess the predictive capability of each modelling strategy. The focus is set on the evolution of the breach discharge and expansion.

The remaining of the paper is organized as follows: the modelling strategies are introduced in Section 2. The field experiments used as test cases are described in Section 3. In Section 4, results are presented and discussed to assess the accuracy and performance of each modelling approach. Finally, conclusions are drawn in Section 5.

2 MODELLING STRATEGIES

2.1 *Lumped model*

We adapted an existing semi-analytical physically-based dam breaching model to the case of fluvial dike breaching (Schmitz et al., 2023). The original model is called DLBreach and was developed by Wu (2013). It is composed of three coupled modules: a hydrodynamic module, a sediment transport module, and a dike morphodynamic module (Figure 1). The sediment transport and dike morphodynamic modules are parts of a so-called "breach evolution module". The flow is assumed uniformly distributed through the entire trapezoidal breach and the breach expansion is symmetric. However, in fluvial configurations, the flow inertia in the main channel direction plays an important role in the breaching process. Laboratory experiments (Rifai et al., 2017), field tests (Kakinuma and Shimizu, 2014) and detailed 2D computations (Charrier, 2015) show that the flow through the breach is not uniformly distributed along the breach width, but rather concentrated in the most downstream part of the breach. This phenomenon induces a greater water velocity near the downstream breach extremity (Charrier, 2015), which leads to more intense erosion at this location. Conversely, limited erosion appears on the upstream extremity, leading to non-symmetrical breach expansion in the case of fluvial dikes (Schmitz et al., 2023).

In our modified implementation of the model of Wu (2013, 2016), we introduced the concept of "effective breach width" to describe the fraction of the total breach width that is effectively used to convey water (Schmitz et al., 2023). Shortly after the breaching onset (i.e., Stage 1 in Rifai et al. (2017)), flow velocity fields along both breach extremities tend to be similar due to the small breach width, leading to a symmetrical breach expansion. During this period, the initial breach expansion description proposed by Wu (2013) is thus used. Once the breach bottom reaches the channel bottom, asymmetrical breach widening is enforced by considering an effective breach width, b_{eff}, equal to half of the total breach width in the present work. This leads to a higher flow velocity, U_b, for a similar breach discharge, Q_b, so that:

$$U_b = Q_b / A_{eff}\,, \tag{1}$$

with $A_{eff} = f(b_{eff})$ the effective breach flow section. Erosion is computed based on this increased velocity and the related effective breach area. Erosion only appears on the downstream breach extremity and breach expansion intensifies in that direction.

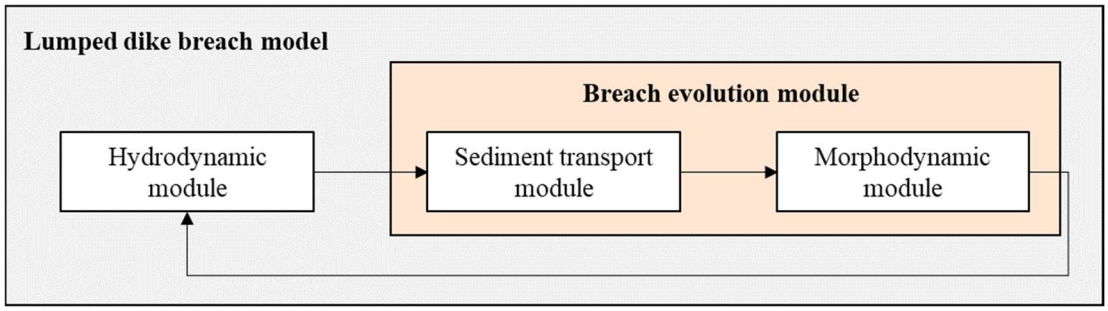

Figure 1. Flow chart of the lumped dike breach model.

2.2 *Dynamic coupling with a 2D-horizontal hydrodynamic model*

Figure 2 provides a flow chart of the second modelling strategy, which consists in dynamically coupling the breach evolution module of the lumped model with WOLF-2D, a 2D-horizontal hydrodynamic model. At each time step, $t_{hydro,n}$, WOLF-2D computes the entire hydrodynamic field. At specific time steps defined by the user, $t_{topo,i}$, the breach evolution module of the lumped model is fed with WOLF-2D hydrodynamic data to compute the breach topography that will be imposed at the next user-specified time step in the hydrodynamic model, $t_{topo,i+1}$. This new topography is sent back to WOLF-2D, which uses a linear interpolation to compute the topography between successive topographies computed by the lumped model. The entire hydrodynamic field is updated accordingly, until reaching the next user-specified time step, $t_{topo,i+1}$. In practice, the hydrodynamic data transmitted by WOLF-2D to the lumped model are the total breach discharge, Q_b, and the mean water depth above the breach, h_{top}, measured along the centerline of the dike crest. In the present case, the breach topography was updated every 5 seconds, i.e., $t_{topo,i+1} - t_{topo,I} = 5$ [s].

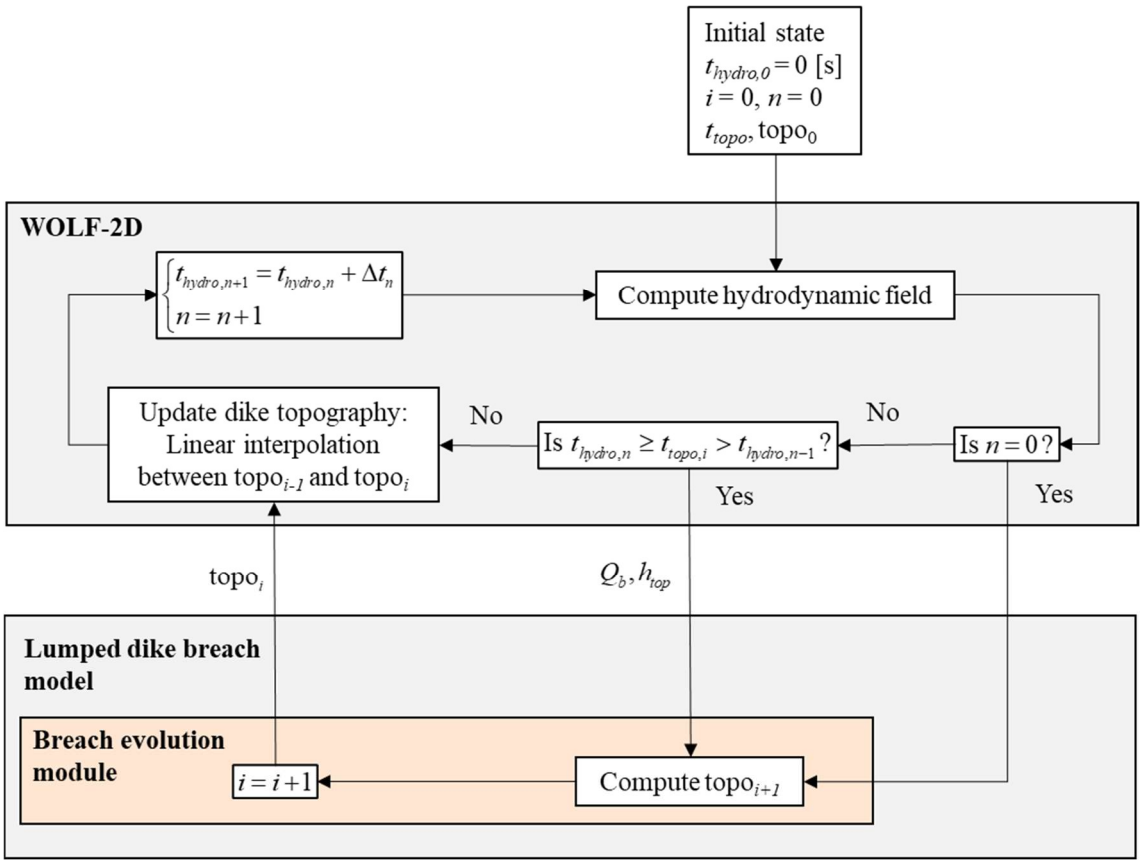

Figure 2. Flow chart of the dynamic coupling between WOLF-2D and the breach evolution module of the lumped dike breach model.

3 CASE STUDIES

3.1 *Experimental setup*

Large scale dike breaching tests were performed on the Chiyoda Test Channel (Tokachi River, Japan) between 2010 and 2011 (Kakinuma et al., 2013). The setup consists of a 735-m-long slightly curved main channel with a bed slope of 1/500 and a variable width (Figure 3). The bottom of the channel is erodible. Here, we consider Tests 1 and 2 of the test campaign.

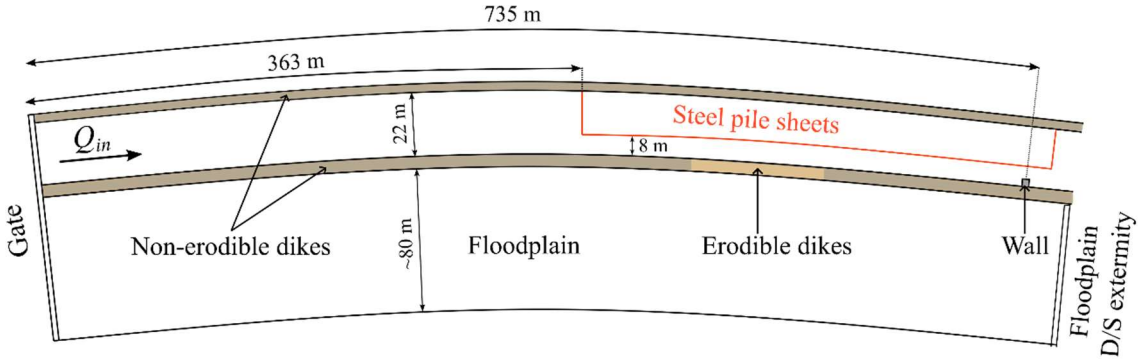

Figure 3. General scheme of the experimental setup.

Over the first 363-m-stretch of the river, both channel sides are limited by a 4-m-high trapezoidal non-erodible dike, whose slopes are equal to 2 (H/V). The channel bottom is 22 m wide over this section. To reach higher water levels using a limited inflow discharge, vertical steel pile sheets were installed on the left side of the rest of the channel to reduce its bottom width to 8 m. A 3-m-high trapezoidal erodible dike was built along part of the right side of the narrow channel (Figure 4). Beside it, an 80-m-large floodplain is present. Its bottom is at the same level as the bottom of the main channel. Finally, there is a wall at the downstream extremity of the main channel to reduce the flow section and regulate the water level. Shortly after that wall, the channel bottom widens to reach 30 m and water is freely released.

The inflow discharge Q_{in} is supplied by an upstream regulating gate and increases progressively until reaching a target inflow discharge of 70 m^3/s in Test 1 and 35 m^3/s in Test 2. During the filling phase, the water level rises in the main channel. Before starting the tests, a 0.5-m-deep notch was dug in the crest of the erodible dike to trigger overtopping. Its top and bottom widths are equal to 3 m and 1 m, respectively. The wall at the channel downstream extremity was designed and the upstream gate operated so that the water level overflows the initial notch bottom by 30 cm. Once the water level overtops the notch, surface erosion and breaching develop.

The main characteristics of the erodible dike and the position of the initial notch center are provided for each tested configuration in Table 1. In both tests, the erodible dike is made of gravel and coarse sand.

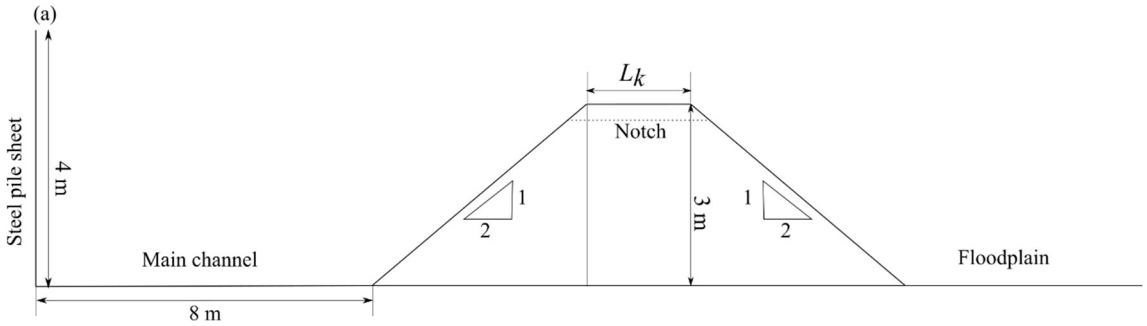

Figure 4. Erodible dike cross section.

Table 1. Tested configurations. L_k = dike crest width; S = dike side slopes (H/V); d_{50} = median grain size of the dike material; F = Froude number in the narrow channel section; x = distance between the upstream gate and the center of the initial notch; w_d = location of the erodible dike section with respect to the initial notch.

Test ID	L_k (m)	S (-)	d_{50} (mm)	Target Q_{in} (m^3/s)	Target F	x (m)	w_d (m)
1	3	2	5.4	70	0.47	463	[-18; 62]
2	3		4.9	35	0.23	583	[-40; 44]

3.2 *Experimental data*

Water levels were recorded in the main channel (along the steel sheet piles) and in the floodplain (50 m from the sheet piles) using radio and hydraulic water gauges. Acceleration sensors were placed in the dike body to monitor its morphological evolution. At the end of each test, when the main channel got empty, the final dike morphology was recorded in more detail using three-dimensional laser scanners.

Water surface velocities were measured by radio flowmeters at the center of the channel. Data were collected every second. Average values over periods of 60 seconds were considered to smoothen the signal. Flow rates were derived from the flow cross-sections and the recorded surface velocities using a corrective factor that considers the non-uniform velocity distribution along the river depth. In both tests, the flow rate was recorded 50 m upstream of the initial notch. Additionally, it was recorded 120 m and 50 m after the notch in Test 1 and Test 2, respectively.

The discharge through the breach was deduced from mass balance applied to a control volume around the breach. The upstream and downstream extremities of the control volume corresponded to the flow rate measurement locations.

3.3 *Parametrization of the case studies in the numerical models*

In both modelling approaches, the adopted geometry is similar to the one displayed in Figure 3, except the slight channel curvature that is discarded. In WOLF-2D, a non-erodible bed with a constant slope of 1/500 is considered in the main channel and the floodplain. The floodplain is 80 m wide and stretches along the entire dike length. A boundary condition on the Froude number is prescribed at the downstream extremity of the floodplain (F = 0.75). The dike breaching event is not expected to be sensitive to this value as the flow through the breach is mostly supercritical. The other extremities of the floodplain are considered as waterproof. A Manning coefficient of 0.023 [s/m$^{1/3}$] is applied to the whole domain, as suggested in the experimental data base. Backwater effect may be considered in the lumped model, but it is discarded here as too little information is available in this region (topography, sediment characteristics…).

The same inflow discharge is used in both modelling strategies. At the beginning of each simulation, no water is present in the domain. The inflow discharge is injected at the upstream extremity of the main channel, i.e., at the gate location. In all tests, the flow measured at the gate is smaller than that measured 50 m upstream from the notch by about 10% on average, i.e., mass conservation is not ensured. The latter discharge was used by Kakinuma and Shimizu (2014) to derive the experimental breach discharge. For this reason, we selected the flow discharge measured 50 m upstream from the initial notch as the inflow discharge in all modellings. A time shift of 9 minutes is applied to take into account the time required for water to leave the gate and reach the position 50 m upstream from the notch. The relevance of this time shift was validated based on numerical tests.

We impose an explicit relation between the water level and the downstream outflow discharge as a downstream boundary condition in both modelling approaches. An experimental downstream rating curve is used to fit the weir discharge coefficient, C_d, in the following relation:

$$Q_{out} = \frac{2}{3} C_d l_w \sqrt{g(h-w)^3}, \quad (2)$$

with Q_{out} the outflow discharge, l_w the width of the weir (i.e., the channel bottom here), g the

gravity acceleration, h the mean water free surface elevation, and w the weir crest elevation (i.e., the channel bed elevation in this case). This relation is applied at the location where the experimental rating curves were measured, i.e., 120 m (Test 1) or 50 m (Test 2) from the initial notch, so that the computational domain is trimmed at this location. No explicit representation of the downstream wall is required in this case as the experimental rating curves are systematically located upstream of it.

4 RESULTS AND DISCUSSION

In this section, results generated by the lumped dike breach model alone and the dynamic coupling between WOLF-2D and the breach evolution module of the lumped model are discussed and compared. Additionally, two alternative approaches were adopted by using the experimental breach width at the dike crest level as an input in the lumped model and WOLF-2D. Those approaches allow focusing on the capability of each model to predict the breach discharge, independently of the performance of the erosion module. In those cases, the observed breach geometry is simplified as a flat bottom and two constant lateral slopes. Also, the breach deepening is obtained by assuming a uniform erosion rate over the entire breach surface because only the breach width at the dike crest level was recorded during the experiments. In practice, a linear interpolation is used between two successive input topographies.

Figure 5 shows the evolution of the breach discharge in the field tests presented in Section 3. All modelling strategies predict the peak discharge with less than 20% error, except the dynamic coupling in Test 1. Both modelling approaches based on the experimental breach topography provide acceptable results, although the lumped model tends to systematically overestimate the peak breach discharge when fed with the experimental breach topography.

When the lumped model computes the breach expansion itself (yellow curves in Figure 5), the results are satisfactory, especially in Test 2. However, the breach width is largely underestimated, i.e., the final breach width is underestimated by 63% and 45% in Tests 1 and 2, respectively. Combining these observations shows that, in this model, the breach conveys too much water for a given breach width, whilst erosion is underestimated for a given breach discharge. This trend is clearly highlighted when the lumped model uses the experimental breach topography as an input, i.e., the peak breach discharge is systematically overestimated. A similar observation holds when considering the dynamic coupling approach. In this case, shallow-water equations are used to compute the flow through the breach. This leads to a smaller breach discharge than what is obtained with the lumped model, which induces an even lower breach widening. Consequently, the breach discharge is largely underestimated as well.

To tackle these limitations, the breach evolution module of the lumped model should be revised so that the computed erosion rates intensify for a given breach width and discharge. A solution may consist in defining in more detail the velocity field through the breach to better calibrate the effective breach width that dictates the breach erosion rate. 3D numerical simulations and laboratory tests could potentially help objectify this characterization and increase the predictive capability of modelling strategies based on the erosion module of the lumped dike breach model.

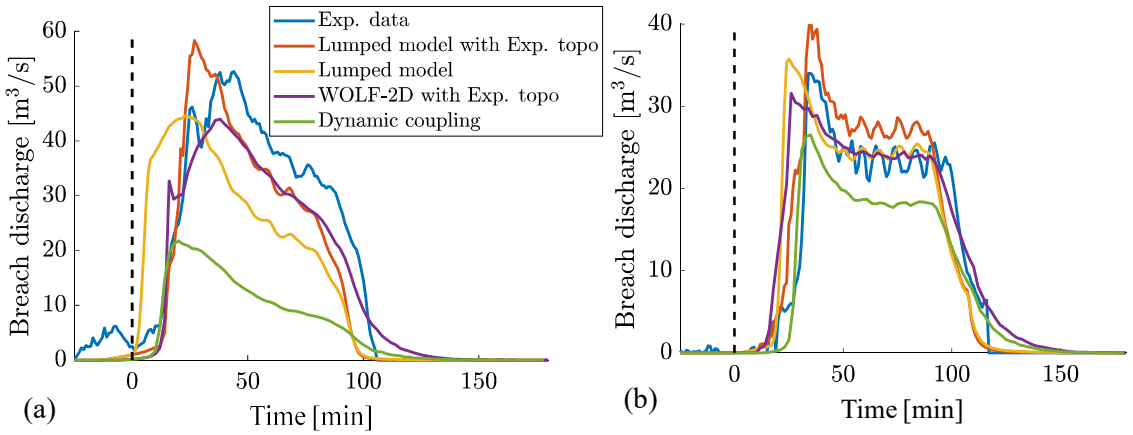

Figure 5. Experimental and numerical breach discharges obtained for Test 1 (a) and Test 2 (b).

5 CONCLUSION

Two modelling strategies were implemented and applied on two field-scale dike breaching experiments. The first one consists in describing the flow and the morphologic evolution of the dike breach using a lumped dike breach model. In the second modelling approach, a 2D hydrodynamic model (WOLF-2D) was dynamically coupled with the breach evolution module of the lumped dike breach model, whose goal was limited to the description of the dike breach topography.

Both models perform well in predicting the breach discharge evolution, although the non-discretized model tends to systematically overestimate the breach flow. Conversely, the breach expansion is poorly predicted by the breach evolution module, which is used in both modelling approaches. In future studies, the focus should be set on the improvement of this module by improving the definition of the breach effective width, i.e., the part of the breach which conveys most of the water and hence controls the breach erosion dynamics.

REFERENCES

Charrier, G., 2015. Etude expérimentale des ruptures de digues fluviales par surverse.

Chen, Z.Y., Ping, Z.Y., Wang, N.X., Yu, S., Chen, S.J., 2019. An approach to quick and easy evaluation of the dam breach flood. Science China Technological Sciences 62, 1773–1782.

Dazzi, S., Vacondio, R., Mignosa, P., 2019. Integration of a Levee Breach Erosion Model in a GPU-Accelerated 2D Shallow Water Equations Code. Water Resources Research 55, 682–702.

De Lorenzo, G., Macchione, F., 2014. Formulas for the peak discharge from breached earthfill dams. Journal of Hydraulic Engineering 140, 56–67.

Hu, P., Ji, A., Li, W., Cao, Z., 2023. Numerical modelling of levee breach with an improved slope-failure operator. Journal of Hydraulic Research 1–13.

Kakinuma, T., Shimizu, Y., 2014. Large-scale experiment and numerical modeling of a riverine levee breach. Journal of Hydraulic Engineering 140.

Kakinuma, T., Tobita, D., Yokoyama, H., Takeda, A., 2013. Levee breach observation at Chiyoda experimental flume, in: 12thInternationalSymposium River Sedimentation (ISRS), IRTCES, Kyoto, Japan.

Lee, K., 2019. Simulation of Dam-Breach Outflow Hydrographs Using Water Level Variations. Water Resources Management 33, 3781–3797.

Li, Y., Chen, A., Wen, L., Bu, P., Li, K., 2020. Numerical simulation of non-cohesive homogeneous dam breaching due to overtopping considering the seepage effect. European Journal of Environmental and Civil Engineering.

Peter, S.J., Siviglia, A., Nagel, J., Marelli, S., Boes, R.M., Vetsch, D., Sudret, B., 2018. Development of Probabilistic Dam Breach Model Using Bayesian Inference. Water Resources Research 54, 4376–4400.

Rifai, I., Erpicum, S., Archambeau, P., Violeau, D., Pirotton, M., El Kadi Abderrezzak, K., Dewals, B., 2017. Overtopping induced failure of noncohesive, homogeneous fluvial dikes. Water Resources Research 53, 3373–3386.

Schmitz, V., Rifai, I., Kheloui, L., Erpicum, S., Archambeau, P., Violeau, D., Pirotton, M., El Kadi Abderrezzak, K., Dewals, B., 2023. Main channel width effects on overtopping-induced non-cohesive fluvial dike breaching. Journal of Hydraulic Research 61, 601–610.

Tsai, C.W., Yeh, J., Huang, C., 2019. Development of probabilistic inundation mapping for dam failure induced floods. Stochastic Environmental Research and Risk Assessment 33, 91–110.

Van Damme, M., 2020. An analytical process-based approach to predicting breach width in levees constructed from dilatant soils. Natural Hazards 101, 59–85.

Wu, W., 2013. Simplified physically based model of earthen embankment breaching. Journal of Hydraulic Engineering 139, 837–851.

Wu, W., 2016. Introduction to DL Breach–A simplified physically based dam/levee breach model. Clarkson University, NY.

Zhong, Q., Wang, L., Chen, S., Chen, Z., Shan, Y., Zhang, Q., Ren, Q., Mei, S., Jiang, J., Hu, L., Liu, J., 2021. Breaches of embankment and landslide dams - State of the art review. Earth-Science Reviews 216.